Nanoscale

Accepted Manuscript

This article can be cited before page numbers have been issued, to do this please use: A. Mahata and B. Pathak, *Nanoscale*, 2017, DOI: 10.1039/C7NR03002A.

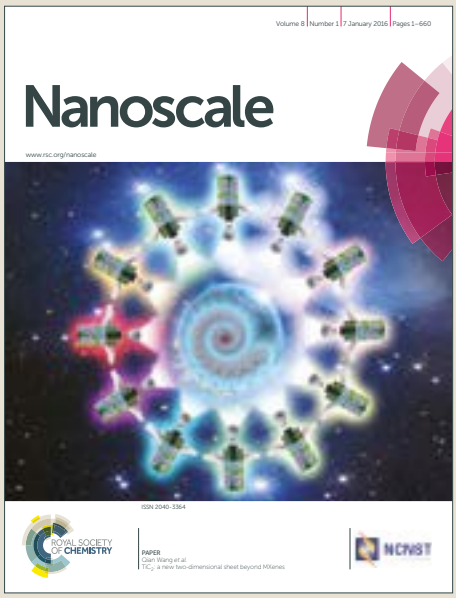

ROYAL SOCIETY OF CHEMISTRY

rsc.li/nanoscale

View Article Online
DOI: 10.1039/C7NR03002A

Bimetallic Core-Based Cuboctahedral Core-Shell Nanocluster for Hydrogen Peroxide (2e$^-$ reduction) over Water (4e$^-$ reduction) Formation: Role of Core Metals

Arup Mahata,[†] Biswarup Pathak[†,#,*]

[†]Discipline of Chemistry, School of Basic Sciences, and [#]Discipline of Metallurgy Engineering and Materials Science, Indian Institute of Technology (IIT) Indore, Indore, Madhya Pradesh 453552, India
Email: biswarup@iiti.ac.in

Abstract:

The designing of an efficient and selective catalyst for hydrogen peroxide (H_2O_2) formation is highly sought due to its importance in industries. Unlike conventional Pd-Au alloy based catalyst, the catalytic activity of three cuboctahedral core-shell nanocluster ($Au_{19}@Pt_{60}$, $Co_{19}@Pt_{60}$ and $Au_{10}Co_9@Pt_{60}$) has been investigated toward H_2O_2 formation and compared that with the pure Pt cuboctahedral NC (Pt_{79}). Much attention has been devoted to thermodynamic and kinetic parameters to find out the feasibility of 2e$^-$ over 4e$^-$ oxygen reduction reaction (ORR) to improve the product selectivity (H_2O vs. H_2O_2). Elementary steps correspond to H_2O_2 formation are significantly improved over $Au_{10}Co_9@Pt_{60}$ nanocluster (NC) than that on the pure, core-shell NCs, periodic surface based catalysts. Furthermore, $Au_{10}Co_9@Pt_{60}$ NC favours H_2O_2 formation via the much desired Langmuir-Hinshelwood mechanism. The potential dependent study shows that the H_2O_2 formation is thermodynamically favourable up to 0.43 V on $Au_{10}Co_9@Pt_{60}$ NC and thus significantly lowers the overpotential for 2e$^-$ ORR process. Besides, the $Au_{10}Co_9@Pt_{60}$ NC is very much selective towards H_2O_2 formation over H_2O formation.

Keywords: Direct hydrogen peroxide formation, Core-shell nanocluster, Reaction Mechanism, Selectivity, Density functional calculations

View Article Online
DOI: 10.1039/C7NR03002A

1. Introduction:

Hydrogen peroxide (H_2O_2) is an environment friendly oxidant that is extensively used in many industrial applications such as in pulp and paper industry, water treatment, chemical synthesis and so on.[1-2] H_2O_2 is currently produced at commercial scale by the indirect process, where anthraquinone is hydrogenated to anthrahydroquinone in the presence of a Pd-catalyst. Then anthrahydroquinone undergoes to an autoxidation to regenerate anthraquinone and H_2O_2 as a by-product.[3] However, this is an expensive recycling process, which produces concentrated H_2O_2. Thus the challenge is to develop an efficient and selective catalyst for H_2O_2 production. In this context, the oxygen reduction process is a promising approach for the direct synthesis of H_2O_2.[4-9]

However, the oxygen reduction reaction (ORR) is a multi-step process. It can either proceed through a two-step two-electron reduction for H_2O_2 formation or via a four-step four-electron reduction for H_2O formation. Pd-Au bimetallic catalysts have been reported as most effective catalysts for the direct synthesis of H_2O_2. The Au component induces "ensemble effect" (particular arrangement of active constituents) and/or "electronic effect" (change in electronic environment of Pd metal), which improve the activity of the Pd based catalyst.[11] Extensive studies have been carried out both in experimentally and theoretically on the Pd-Au based catalyst for H_2O_2 synthesis[11-17]. However, there are major problems toward product selectivity over the Pd-based catalysts.[18] The synthesis process undergoes through low product (H_2O_2) selectivity due to the competition between $2e^-$ (H_2O_2 formation) vs. $4e^-$ (H_2O formation) reduction reaction. Besides, the Pd-based catalyst binds H_2O_2 strongly, which in turn favours H_2O_2 decomposition to H_2O and O_2 via a disproportionation reaction or via a hydrogenation reaction to H_2O.[4,19-21] Further, the dissociative adsorption of a hydrogen molecule is sluggish on Pd-based catalysts.[22] In fact, previous experimental studies reported the poor performance of a

View Article Online
DOI: 10.1039/C7NR03002A

Pd/C catalyst towards hydrogen oxidation reaction (HOR) while compared to Pt/C or Pd-Pt/C based catalysts.[23-24] So, a slow reaction occurs between the adsorbed hydrogen atoms and oxygen molecules on a Pd-based catalyst to proceed through the typical Langmuir-Hinshelwood mechanism for H_2O_2 formation.[14,25] Thus, the performance of a catalyst for H_2O_2 production depends on three important steps: (i) H_2 oxidation (HOR) (ii) O_2 hydrogenation, and (iii) H_2O_2 formation. Interestingly, Pt is one of the best catalysts for HOR and O_2 hydrogenation.[26-27] Therefore, there is a high possibility that the ORR reaction may proceed through the typical Langmuir-Hinshelwood mechanism when catalyzed by a Pt-based catalyst. However, Pt based catalysts are not preferred over Pd based catalysts for H_2O_2 synthesis. This is due to the fast kinetics for OH and H_2O formation on the Pt based catalysts than that on the Pd based catalysts.[28] Besides, the indirect O-O bond dissociation is favourable over Pt catalysts.[26-27,29-30] Therefore, Pt is not a selective catalyst for H_2O_2 formation.[31] However, Pt-based catalysts can be selective for H_2O_2 formation if the OOH hydrogenation (H_2O_2 formation) is preferred over the OOH dissociation.

Nørskov and co-workers reported that the binding energy of *O and *OH on the metal surface should neither be strong nor weak, so that the reaction species can be desorbed easily from the catalyst surface as well as can stabilize the intermediate.[32] Similarly, OOH is an important intermediate for H_2O_2 formation. Therefore, it should bind on the catalyst surface in an optimal range so that it can facilitate the OOH formation as well as the OOH hydrogenation. The Pt-based catalyst with a mixed alloy core (with strong and weak binding) could be an excellent option for the optimal binding of OOH. Now, a surface that binds O-atom in optimal range can also be expected to bind OOH linearly, as both the adsorbates binds the surface via the O-atom.[33]

View Article Online
DOI: 10.1039/C7NR03002A

Therefore, we have chosen Co and Au as a mixed-alloy core from the two opposite sides of the volcano curve of O-binding energy to get the optimal binding of OOH.[32,33]

Apart from the composition of a catalyst, the morphology of a bi-metallic catalyst is also very important for their catalytic activity. Bi-metallic catalysts have been often designed as skeleton-surface,[34] skin-surface,[35] mixed alloy[36] and core-shell structures.[37] Among them, core-shell based catalysts are very promising due to the easy tunability of inside core and their facile synthetic route.[38] For this, three cuboctahedral core-shell NCs (M_{19}@Pt_{60}; M= Co, Au and Au+Co) are modelled to study the full reaction mechanism for H_2O_2 formation. Moreover, core shell NCs are modelled to understand the role of core metal for improving the selectivity and efficiency for H_2O_2 formation. For comparisons, our results are compared with the available data on the conventional bulk Pd(111), Au(111), Pd-Au(111) and Pt(111) surfaces. Besides, kinetic analysis is performed to gain more insights into the rate of reaction and product selectivity (H_2O_2 vs. H_2O). A potential dependent reaction free energy diagram has been established to understand the thermodynamic feasibility of such elementary reactions as such electrochemical reaction happens under an applied potential. Moreover, a detailed investigation based on the structural change and electronic properties is performed to gain more insights into the role of core-composition towards catalytic activity. Therefore, in this work, we have attempted to provide a significant insight into the designing of an efficient core-shell based Pt catalyst for H_2O_2 over H_2O formation.

2. Model and Computational Details:

The core-shell nanoparticles have been often theoretically modelled using the slab model. However, the effect of low-coordinated sites (twin boundaries, edge and vertex atoms) of nanoparticle can't be mimicked using slab model. These highly unsaturated sites possess higher

View Article Online
DOI: 10.1039/C7NR03002A

d-band energies, which influences the overall activity of the nanoparticles. Basically, the slab model resembles a larger nanoparticle.[30] Therefore, cluster model study with well-defined facets can only provide the real scenario about the experimental situation. The Pt_3M (M = Co, Fe, Ni, Ti) based surfaces are well known for excellent oxygen reduction activity.[39-40] However, here we have designed three types of core-shell NCs (~1.5 nm) maintaining the same ratio (3:1) of Pt and M (M= Au, Co, and Au+Co). Therefore, we have modelled the $M_{19}@Pt_{60}$ NC in the shape of a cuboctahedral geometry, where the core and shell structures contain 19 and 60 atoms, respectively. The $M_{19}@Pt_{60}$ NC (Figure 1a) is modelled with eight (111) and six (001) facets. In reality, (111), (002) and/or (200) planes are mainly observed in the XRD patterns of experimentally synthesized Pt NC.[41] As the (200)/(002) has the same pattern as in (100)/(001), we have considered cuboctahedral NC enclosed by (111) and (001) facet to model similar to experimentally synthesized NC. Furthermore, several groups have previously reported the superior catalytic activity of the cuboctahedral NC over octahedral, cubic, icosahedral NC. Wu et al.[42] investigated a series of Pt_3Ni NCs with exposed (111) and (100) facets and reported that the truncated-octahedral or cuboctahedral NCs with highly exposed (111) facets increase the ORR mass activity by 1.8 times than that of the octahedral NCs. In another experimental study, it has been reported that the hexagonal Pt nanoparticle with (100) and (111) exposed facets displays the highest ORR activity compared to the sphere (no preferential facets), tetrahedral/octahedral (with (111) facets) and cubic (with (100) facets) NCs.[43] In addition, many experimental reports concluded that cuboctahedral NC shows higher ORR activity compared to other geometries.[44] In fact, we have theoretically demonstrated that a cuboctahedral NC with (111) and (100) facets is more active than that of a similar size octahedral (111) NC.[45] Therefore, based on these findings, we have chosen cuboctahedral motif as our modelled catalyst.

View Article Online
DOI: 10.1039/C7NR03002A

A (3 × 3) supercell of periodic AuCo@Pt(111) surface is modelled [Figure S1a] to minimize the lateral interactions between the repeating images. As the NCs contain three atomic layers, therefore we have modelled a three-layer slab for a vis-à-vis comparison between cluster and slab model. In the slab model, the top layer is of completely Pt atoms, whereas the bottom two layers are made of Au-Co alloy maintaining the ratio of 1:1 between Au and Co atoms. For $Au_{19}@Pt_{60}$, $Co_{19}@Pt_{60}$ NCs, the 19 atoms core composed of Co and Au atoms, respectively. Such Au@Pt[46] and Co@Pt[47] core-shell NCs have been experimentally synthesized. However for $Au_{10}Co_9@Pt_{60}$, we have modelled a mixed core of Au and Co atoms with ~1:1 atomic ratio to maintain the maximum symmetry of the core structure (Figure 1d and Figure S1b). All the atoms are fully relaxed by setting the convergence criteria for total energy and forces at 10^{-4} eV and <0.02 eV/Å, respectively. The optimized $Au_{10}Co_9@Pt_{60}$ NC has a near D2h symmetry and is a local minimum energy structure.

In order to investigate the thermodynamic stability of the core-shell NCs, we have calculated segregation energy for $Au_{19}@Pt_{60}$, $Co_{19}@Pt_{60}$ and $Au_{10}Co_9@Pt_{60}$ NCs. Segregation energy (E_{seg}) has been calculated using the following equation:

$$E_{seg} = E_{seg\text{-}NC} - E_{NC}$$

where $E_{seg\text{-}NC}$ is the total energy of the NC after exchanging the core-atom with a shell Pt-atom and E_{NC} is the total energy of the core-shell NC.

Therefore, positive segregation energy represents that Pt atom prefers to stay in the shell layer, whereas negative segregation energy represents that Pt atom prefers to stay in the core. The optimized geometries of the segregated structures have been shown in Figure S2. Our results show that the core Au atoms prefer to exchange (-0.18 eV) with the Pt shell atoms in $Au_{19}@Pt_{60}$ NC. In contrast, Co atom prefers to stay in the core with segregation energy of 1.86 eV. Previous

View Article Online
DOI: 10.1039/C7NR03002A

study[48] on the 55-atom NC also reported about the shell preference of Au atoms and core preferences of Co atoms though experimentally Au@Pt NCs have been synthesized.[46-47] Interestingly, the negative segregation energy of Au atom (-0.18 eV as pure core) becomes negligible (-0.03 eV) in case of the mixed core (Au+Co), whereas the positive segregation energy of Co atom (1.86 eV as pure core) reduces to 0.91 eV in case of the mixed core (Au+Co). This might be due to the strong bonding between Au and Co atoms. The ORR mechanism has been studied on the Pt(111) facet of the NCs. It has been previously reported (theoretically as well as experimentally) that the Pt(111) is the mostly exposed and active facet for ORR.[45, 49-52]

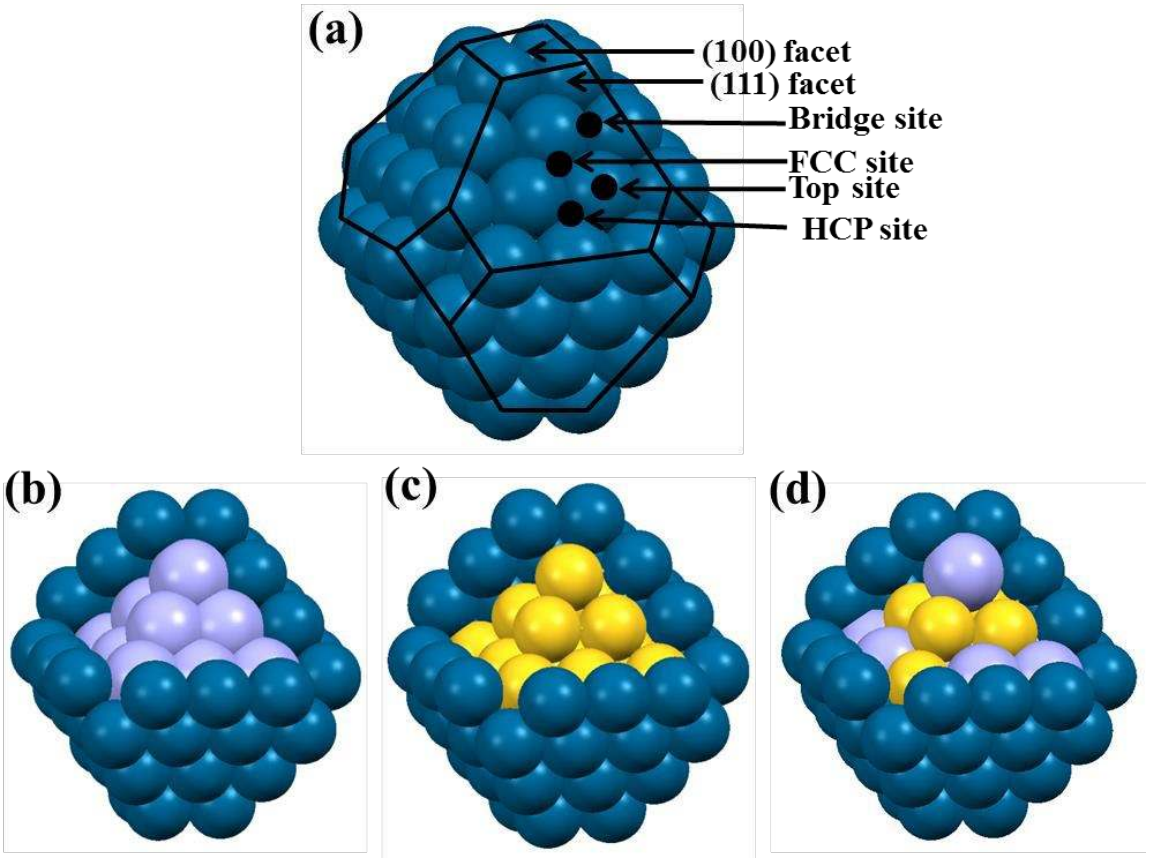

Figure 1: Cuboctahedral (a) pure Pt and (b-d) core-shell (M_{19}@Pt_{60}) NCs enclosed with eight (111) and six (001) facets. Here light purple, yellow and blue colour balls represent cobalt, gold (M) and platinum metal atoms, respectively.

View Article Online
DOI: 10.1039/C7NR03002A

The first-principles calculations are performed using a projector augmented wave (PAW)[53] method as implemented in the Vienna Ab initio Simulation Package (VASP).[54-56] The exchange-correlation potential is described by using the generalized gradient approximation of Perdew-Burke-Ernzerhof (GGA-PBE).[57] Projector augmented wave (PAW) method is employed to treat interactions between ion cores and valance electrons.[53] We have included Grimme's D3-type[58] of semiempirical method to include the dispersion energy corrections for van der Walls interactions. The climbing nudged elastic band (CI-NEB) method[59] is used to locate the transition state. The detailed computational part has been provided in Supporting Information (Text S1).

3. Results and Discussion:

3.1 Adsorption

There are four possible catalytic sites (Figure 1a) on the (111) facet of NC: (i) top, (ii) bridge, (iii) face centered cubic (fcc) and (iv) hexagonal close packed (hcp). Table 1 presents most stable site and its respective binding energy for all the intermediates. For comparisons, we have tabulated adsorption energies of all the intermediate species on the (111) facet of the pure Pt NC[45] (Pt_{79}). Figure S3 shows the adsorption type of all the intermediates. Interestingly, the preferred binding sites are same for all the adsorbates except for OH. OH preferably binds at the top site of the (111) facet of Pt_{79}, $Co_{19}@Pt_{60}$ and $Au_{10}Co_9@Pt_{60}$ NCs, whereas it is most stable at the bridge site on the (111) facet of $Au_{19}@Pt_{60}$ NC. Hydrogen molecule is not stable on the $Au_{19}@Pt_{60}$ and $Au_{10}Co_9@Pt_{60}$ NCs, rather it dissociates into atomic hydrogen upon adsorption. Our spin polarized study shows that the adsorbed $*O_2$ (tilted) has a total magnetic moment of 0.82, 0.74 and 0.81 μB while adsorbed on the Pt(111) facet of $Au_{19}@Pt_{60}$, $Co_{19}@Pt_{60}$ and $Au_{10}Co_9@Pt_{60}$ NCs, respectively. On the other hand, the adsorbed *O is a nonmagnetic one

View Article Online
DOI: 10.1039/C7NR03002A

while adsorbed on the NCs surface. This is very much consistent with the previous reports on $*O_2$ and *O adsorbed on the periodic Pt(111) surfaces.[60]

Table 1: Preferred binding sites, binding energies (eV) of the most stable ORR intermediate species on the Pt(111) facet of the NCs and periodic Pt(111) surface. Here t, b and f denote top, bridge and fcc sites, respectively. Respective Values on the Pt_{79} NC and periodic Pt(111) have been taken from reference number 45 and 10, respectively.

Adsorbed Species	**Co_{19}@Pt_{60}**	**Au_{19}@Pt_{60}**	**$Au_{10}Co_9$@Pt_{60}**	**Pt_{79}**	**Periodic Pt (111)**
$*O_2$	-0.01 (t)	-0.45 (t)	-0.22 (t)	-0.60 (t)	-0.67
*O	-4.42 (f)	-5.51 (f)	-5.40 (f)	-5.19 (f)	-4.42
*OH	-1.99 (t)	-3.35 (b)	-2.12 (t)	-2.49 (t)	-2.37
*OOH	-0.95 (b)	-1.26 (b)	-1.12 (b)	-1.40 (b)	-1.15
$*H_2O_2$	-0.21 (b)	-0.26 (b)	-0.28 (b)	-0.34 (b)	-0.30
$*H_2O$	-0.08 (t)	-0.14 (t)	-0.22 (t)	-0.23 (t)	-0.26
*H	-2.47 (f)	-2.98 (f)	-2.81 (f)	-2.80 (f)	-2.77
$*H_2$	-0.05 (t)	-	-	-0.34 (t)	-

Furthermore to take into account the adsorption behaviour at the low-coordinated site, we have calculated the adsorption energies of all the possible reaction species at the edge site of the $Au_{10}Co_9$@Pt_{60} NC and the values have been provided at the Supporting Information (Table S1). It is very interesting to note that all the species except *O bind strongly on the edge position compared to the (111) facet, which is due to the high unsaturation of edge atoms. Besides, the strong adsorption energy of the end products ($*H_2O$ and $*H_2O_2$) at the edge site poisons the catalyst surface. More importantly, the H_2 molecule doesn't undergo dissociative adsorption on the edge sites as in the case of (111) facet, thus rendering the possibility of undergoing the reaction through the typical Langmuir-Hinshelwood mechanism.

View Article Online
DOI: 10.1039/C7NR03002A

In addition, to check the effect of compositional change towards reactivity, we have modelled a NC with 9 Au and 10 Co atoms ($Au_9Co_{10}@Pt_{60}$) as core atoms. The adsorption energy of all the reaction intermediates have been studied on the $Au_9Co_{10}@Pt_{60}$ NC's surface and the values have been provided in the Supporting Information (Table S2). Our results show that only *O adsorb weakly on the $Au_9Co_{10}@Pt_{60}$ NC's facet, whereas the effect is negligible on the other reaction intermediates and products ($*O_2$, *OH, *OOH, $*H_2O$ and $*H_2O_2$). Therefore, different composition of 1:1 ratio does not change the adsorption energy.

3.2 ORR Mechanism

O_2 hydrogenation vs. dissociation:

There are two competing pathways (Scheme 1) for the adsorbed $*O_2$ for the ORR. Either the adsorbed O_2 will dissociate into atomic oxygen (*O) or it will be hydrogenated to *OOH. For H_2O_2 formation, O_2 hydrogenation is important over O_2 dissociation. Previous studies on the bulk metal surfaces[10,61], NCs[45] and nanocage[10] show that $*O_2$ molecule orients itself from the superoxo to tilted conformer before its activation. Therefore, we have calculated activation barriers for $*O_2$ dissociation (step 1) and $*O_2$ hydrogenation (step 2) while $*O_2$ adsorbed in the tilted pattern. The direct $*O_2$ bond dissociation is an exergonic process irrespective of the catalyst. However, the calculated barriers are low over the $Co_{19}@Pt_{60}$ (0.07 eV) and $Au_{10}Co_9@Pt_{60}$ (0.06 eV) NCs, whereas it is high (0.76 eV) on the $Au_{19}@Pt_{60}$ NC.

View Article Online
DOI: 10.1039/C7NR03002A

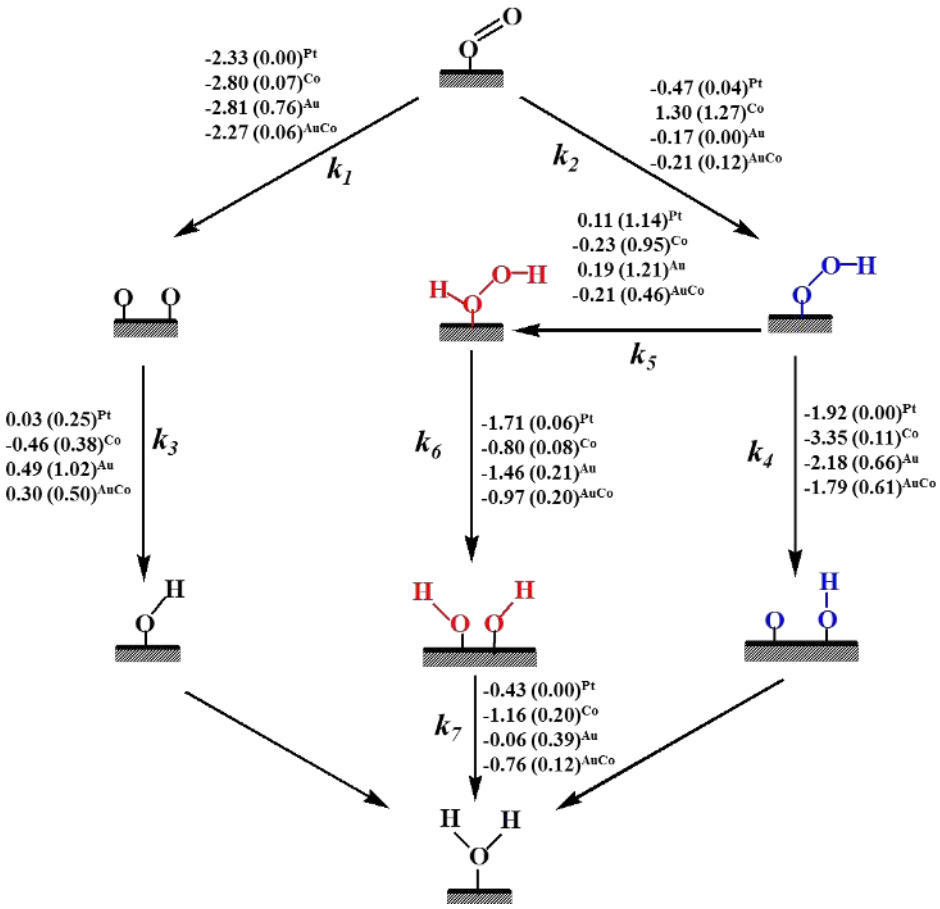

Scheme 1: Reaction free energies (eV) and activation barriers (eV, in parenthesis) are presented for all the possible elementary steps for H_2O_2 and H_2O formation over the NCs surface. Here, Pt, Au, Co and AuCo in the superscripts represent the Pt_{79}, $Au_{19}@Pt_{60}$, $Co_{19}@Pt_{60}$ and $Au_{10}Co_9@Pt_{60}$ NCs, respectively.

On the other hand, O_2 hydrogenation (step 2) shows a little different pattern on the NCs. The calculated activation barriers for O_2 hydrogenation are very low on the pure Pt_{79} (0.04 eV) and $Au_{19}@Pt_{60}$ (barrierless) NCs, whereas the barrier is little high (0.12 eV) on the $Au_{10}Co_9@Pt$ NC. O_2 hydrogenation has an activation barrier of 1.27 eV when catalysed by $Co_{19}@Pt_{60}$ NC. This is interesting that Au core based NC favours O_2 hydrogenation, whereas Co core NC does not favour hydrogenation. Previous studies on the periodic Pd(111) and Pd(111) with Au-Pd mixed sub-surface alloy also reported that the presence of Au metal lowers the activation barrier for O_2

View Article Online
DOI: 10.1039/C7NR03002A

hydrogenation, whereas increases the O_2 dissociation barrier.[14] However, Co-based platinum catalysts show enhanced ORR activity due to favourable $*O_2$ dissociation over *OOH formation.[62] It is interesting to find out that the O-O dissociation barriers are very close on $Co_{19}@Pt_{60}$ and $Au_{10}Co_9@Pt_{60}$ NCs, whereas O_2 hydrogenation barriers are very close on $Au_{19}@Pt_{60}$ and $Au_{10}Co_9@Pt_{60}$ NCs. Therefore, the dissociation process is much influenced due to the presence of core Co atoms, whereas hydrogenation process is affected due to the presence of core Au atoms. It has been reported that strong interaction between Pt and O_2 molecule lowers the O_2-dissociation barrier.[63] But this is contradictory to our results (Scheme 1; Table S3), as $Au_{19}@Pt_{60}$ NC binds O_2 molecule strongly. However, Au core NC favours $*O_2$ hydrogenation over dissociation. Though the adsorption energy is far from the optimal adsorption values as proposed by Nørskov and co-workers[32] and it is very less compared to that on the periodic Pt(111) however, it will be interesting to find out the underlying reason behind the favourable O_2-dissociation on $Co_{19}@Pt_{60}$ NC despite its weak interaction with oxygen molecule. For this, we have carefully investigated Bader atomic charges, vibrational frequencies, and structural parameters of $*O_2$ adsorbed NCs. Our calculated average Bader atomic charges on Pt(111) facet atoms are -0.12 |e|, -0.04 |e|, and -0.01 |e| on $Co_{19}@Pt_{60}$, $Au_{10}Co_9@Pt_{60}$ and $Au_{19}Pt_{60}$ NCs, respectively. It shows that the surface Pt atoms are more electronegative in the case of $Co_{19}@Pt_{60}$. This could be due to the fact that platinum is more electronegative than cobalt, whereas Au has a similar electronegativity as in Pt.[64] On the other hand, the negative charges on adsorbed O-atom of $*O_2$ are -0.172 |e,| -0.148 |e| and -0.150 |e| on $Co_{19}@Pt_{60}$, $Au_{19}Pt_{60}$ and $Au_{10}Co_9@Pt_{60}$ NCs, respectively. Therefore a considerable amount of charge is transferred to π*-orbital of $*O_2$, which subsequently facilitates the O-O bond dissociation. This can be further confirmed from *O-O bond distances. The *O-O bond distances are 1.28, 1.27 and 1.27 Å in

View Article Online
DOI: 10.1039/C7NR03002A

$Co_{19}Pt_{60}$, $Au_{19}Pt_{60}$ and $Au_{10}Co_9@Pt_{60}$, respectively. Besides, the calculated *O-O vibrational (stretching) frequencies of $*O_2$ are 1239, 1254 cm^{-1}, 1285 cm^{-1} on $Co_{19}Pt_{60}$, $Au_{19}Pt_{60}$ and $Au_{10}Co_9@Pt_{60}$ NCs, respectively. Our density of states analysis (Figure 2) shows that the Fermi level is highly populated while $*O_2$ adsorbed on $Co_{19}@Pt_{60}$ than on $Au_{10}Co_9@Pt_{60}$ and $Au_{19}@Pt_{60}$ respectively. Therefore, the population in antibonding states of oxygen, instead of its adsorption behaviour, controls the dissociation kinetics. This behaviour is very much different from the previous ORR studies on the alloy-based Pt(111) surface, where the Pt-O bonding nature has been attributed for O-O bond dissociation process. Therefore, we propose that electropositive core metals can induce more negative charge on surface Pt atoms, which in turn favour O_2-dissociation. Similarly, electronegative core metals will induce positive charge on surface Pt atoms, which may slow down O_2-dissociation process and can improve product (H_2O_2) selectivity.

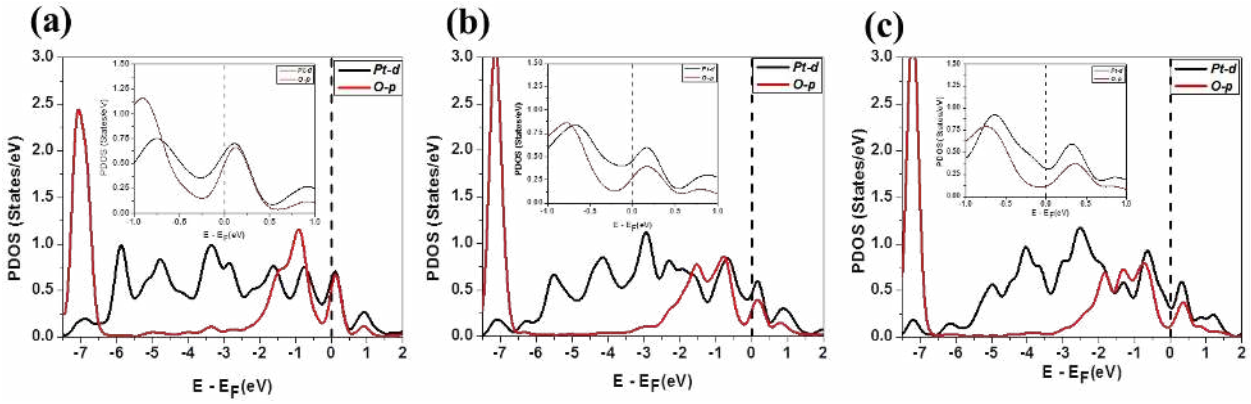

Figure 2: Projected density of states (PDOS) of $*O_2$ adsorbed (a) $Co_{19}@Pt_{60}$, (b) $Au_{10}Co_9@Pt_{60}$, and (c) $Au_{19}@Pt_{60}$, respectively. The inset pictures show the closer view in a smaller energy region.

View Article Online
DOI: 10.1039/C7NR03002A

Xu et al.[65] has reported that Au content Pd-Au catalyst increases the selectivity towards H_2O_2 formation. In fact, it has been experimentally demonstrated that Au nanocluster favours two-electron reduction (H_2O_2 formation) over four-electron reduction (H_2O formation).[66] Therefore, it is expected that Au favours O_2 hydrogenation over dissociation. Moreover, it has been experimentally reported that Au prevents the formation of Pt–OH species on Pt-Au alloy structure and thus allows Pt to act efficiently in the electrocatalytic process.[67] Therefore, Au atoms inhibit the hydrogenation of O-atom (OH formation). Furthermore, it has been experimentally demonstrated that Co helps towards weakening the O-O bond of oxygen molecule, which subsequently helps the ORR to proceed through $4e^-$ reduction.[68] In another study on Co-Pt binary nanoparticles, it has been reported that Co atoms helps toward the cleavage of O-O bond in O_2 molecule.[62] Therefore, our findings agree well with the experimental findings. The previously reported activation barriers for O_2-hydrogenation on the periodic Pd(111) (0.89[14], 0.80 eV[15]), Au(111) (0.20 eV[69]) and Pd-Au(111) (0.53 eV[14]) are very much higher than that on $Au_{10}Co_9@Pt_{60}$ NC (0.12 eV). Therefore, $Au_{10}Co_9@Pt_{60}$ NC could be a selective catalyst for H_2O_2 formation.

H_2 activation:

The direct synthesis of H_2O_2 is believed to be processing via the Langmuir-Hinshelwood mechanism.[14,25,65,70] Thus, two successive hydrogenation reactions are important. Thus the reaction intermediate and hydrogen should be in close proximity. Now, the ease of available atomic *H determines the feasibility of the hydrogenation reaction. In fact, previous experimental studies[71-72] reported the indispensable role H_2 dissociation over the catalyst surface for H_2O_2 synthesis. We find that hydrogen molecule adsorbs very weakly on the $Co_{19}@Pt_{60}$ NC, whereas it dissociates into atomic hydrogen on the $Au_{19}@Pt_{60}$ and $Au_{10}Co_9@Pt_{60}$ NCs. Therefore

View Article Online
DOI: 10.1039/C7NR03002A

the hydrogenation of O_2 molecule is easier on $Au_{19}@Pt_{60}$ and $Au_{10}Co_9@Pt_{60}$ NCs compared to that on $Co_{19}@Pt_{60}$ NC. The ease of H_2 dissociation is high due to the strong adsorption behaviour of *H on the $Au_{19}@Pt_{60}$ (-2.98 eV) NC. However, *H adsorption energy on $Au_{10}Co_9@Pt_{60}$ (-2.81 eV) is neither strong nor weak as on $Co_{19}@Pt_{60}$ (-2.47 eV). Thus $Au_{10}Co_9@Pt_{60}$ NC binds *H in the ideal energy range and therefore, $Au_{10}Co_9@Pt_{60}$ NC is found to be a very potential candidate for O_2 hydrogenation as well as H_2 activation.

***OOH hydrogenation vs. dissociation:**

The adsorbed *OOH may further undergo hydrogenation or dissociation. This may lead toward formation of H_2O_2 (two-electron reduction) or H_2O (four-electron reduction), respectively. Therefore, this is a very important step in terms of product selectivity. Our calculated activation barriers for *OOH hydrogenation (step 5) are 1.14, 0.95, 1.21 and 0.46 eV over the Pt_{79}, $Co_{19}@Pt60$, $Au_{19}@Pt_{60}$ and $Au_{10}Co_9@Pt_{60}$ NCs surface, respectively. On the other hand, *OOH dissociation is a barrierless process on Pt_{79} NC, whereas the dissociation barriers are 0.11, 0.66 and 0.61 eV on the $Co_{19}@Pt_{60}$, $Au_{19}@Pt_{60}$ and $Au_{10}Co_9@Pt_{60}$ NCs, respectively. Thus, the inclusion of Au as a core metal suppresses the dissociation tendency of *OOH (*OOH → *O + *OH) and thus favours H_2O_2 formation. In a study on the Pd-Au alloy, Ham et al. also showed that the presence of Au atoms in the surroundings of Pd has a significant effect towards lowering the O_2-hydrogenation barrier.[16] Moreover, *OOH dissociation is more favored than *OOH hydrogenation (Scheme 1) on Pt_{79}, $Co_{19}@Pt_{60}$ and $Au_{19}@Pt_{60}$ NCs, whereas *OOH hydrogenation is favoured over *OOH dissociation on $Au_{10}Co_9@Pt_{60}$ NC. In fact, our calculated rate constant values (Table S4) on $Au_{10}Co_9@Pt_{60}$ NC also suggest that ratio of OOH hydrogenation (k_5) is ~10^3 times higher that OOH dissociation (k_4). Therefore, a mixed Au+Co

View Article Online
DOI: 10.1039/C7NR03002A

alloy core favours two-electron reduction for the formation of H_2O_2 than the respective mono metallic cores.

On $Co_{19}@Pt_{60}$ NC, the *OOH formation (1.27 eV) as well as *OOH hydrogenation (0.95 eV) are not favoured as both these steps require a high activation barrier. Therefore, H_2O_2 formation is very much unlikely on the (111) facet of $Co_{19}@Pt_{60}$ NC. Moreover, it is noteworthy that first hydrogenation step (OOH formation) is a barrierless process on the $Au_{19}@Pt_{60}$ NC, whereas the subsequent hydrogenation step (H_2O_2 formation) requires a high activation barrier (1.21 eV). Therefore, despite the barrierless OOH formation step, $Au_{19}@Pt_{60}$ NC can't promote H_2O_2 formation. In contrast, the mixed alloy core requires a low activation barrier for *OOH (0.12 eV) and H_2O_2 (0.46 eV) formation. Moreover, both the reactions are thermodynamically favourable.

***H_2O_2 dissociation vs. desorption**

Apart from the possibility of H_2O_2 formation, its subsequent dissociation and desorption are important to understand the complete reduction process. In the dissociation process, *H_2O_2 dissociates into *OH, which can further undergoes hydrogenation for the formation of H_2O. Therefore, the desorption of H_2O_2 prior to its dissociation will improve product selectivity. The *H_2O_2 dissociation barriers (step 6) are low on the Pt_{79} (0.06 eV) and $Co_{19}@Pt_{60}$ (0.08 eV) NCs; showing a similar trend as with O_2 and *OOH dissociation. Besides, our calculated rate constant values (Table S4) suggest that H_2O_2 dissociation is very much favourable on $Co_{19}@Pt_{60}$ NC compared to that on $Au_{19}@Pt_{60}$ and $Au_{10}Co_9@Pt_{60}$ NCs. Interestingly, *H_2O_2 dissociation is not affected due to the presence of mixed core in $Au_{10}Co_9@Pt_{60}$ NC than that on $Au_{19}@Pt_{60}$. It suggests that Au plays a significant role toward suppressing the dissociation process. A similar trend has been also found for OOH dissociation (step 4). Therefore, Pt_{79} and $Co_{19}@Pt_{60}$ NCs

View Article Online
DOI: 10.1039/C7NR03002A

can't promote H_2O_2 production. Interestingly, H_2O_2 dissociation barriers are higher over $Au_{19}@Pt_{60}$ (0.21 eV) and $Au_{10}Co_9@Pt_{60}$ (0.20 eV) NCs than that on pure Pt_{79} (0.06 eV) and $Co_{19}@Pt_{60}$ (0.08 eV) NCs. Although the dissociation barrier of H_2O_2 (0.20 eV) is lower than the H_2O_2 formation (0.46 eV) on $Au_{10}Co_9@Pt_{60}$ NC, the activation barrier (0.46 eV) is sufficient enough to promote the desorption process of weakly bind H_2O_2 rather than favouring its dissociation.

***OH formation:**

The direct O-O bond dissociation followed by hydrogenation leads to the formation of *OH (step 3). The *OH formation is a rate determining step for ORR. Besides, it can be an important factor to understand product selectivity as it may favour H_2O formation over H_2O_2 reduction. The *OH formation (step 3) is an endergonic process over $Au_{19}@Pt_{60}$ (0.49 eV) and $Au_{10}Co_9@Pt_{60}$ (0.30 eV) NCs, whereas it is an exergonic process (-0.46 eV) over $Co_{19}@Pt_{60}$ NC surface. The activation barriers for *OH formation are 0.38, 1.02 and 0.50 eV over $Co_{19}@Pt_{60}$, $Au_{19}@Pt_{60}$ and $Au_{10}Co_9@Pt_{60}$ NCs, respectively. Therefore, Au can be used as a core metal to reduce the possibility of OH formation. To understand this, we have calculated d-band center position of the (111) facet atoms of the NCs. The calculated d-band center energies are -2.50, -2.16, -2.70 and -2.53 eV for Pt_{79}, $Au_{19}@Pt_{60}$, $Co_{19}@Pt_{60}$ and $Au_{10}Co_9@Pt_{60}$, respectively. In general, an upward shift in the d- band center with respect to the Fermi energy results in an upward shift in their anti-bonding states. This leads to less occupancy in the anti-bonding states, which in turn strengthens the bond strength. In this way, Nørskov and co-workers developed a linear relationship between electronic structure, adsorption energies and reaction free energies. Therefore, the strong binding of *O doesn't lead to its easy desorption/migration for the formation of *OH. As a result, the OH formation step becomes less favourable over the core-

View Article Online
DOI: 10.1039/C7NR03002A

shell NCs, where the core metal binds O-atom strongly. This phenomenon is in good agreement with the 'ligand effect' proposed by Nørskov and co-workers.[73] Previously, Henkelmann and co-workers concluded that O-binding affinity and OH formation can be tuned by changing the core composition of the core-shell (M@Pd where M=Pd, Cu) nanoparticles.[74] Previous study reported activation barriers of *OH formation are 0.78 and 0.93 eV on the periodic Pt(111) and Au@Pt(111) surface, respectively.[75] It indicates that alloying with Au increases the activation barrier for *OH formation. Therefore, our core-shell NCs models report a similar trend as reported using slab models.

On the other hand, Co atoms of $Au_{10}Co_9@Pt_{60}$ have less influence on hydrogenation process (step 3) than that due to the presence Au. So, water formation is difficult on $Au_{10}Co_9@Pt_{60}$ NC as OH formation is slow over $Au_{10}Co_9@Pt_{60}$ NC. More importantly, the OH formation barrier on $Au_{10}Co_9@Pt_{60}$ NC is 0.50 eV, which is higher than the highest barrier (0.46 eV) for $2e^-$ reduction (H_2O_2 formation). Furthermore, H_2O_2 formation is an exergonic (-0.21 eV) reaction, whereas OH formation is an endergonic reaction (0.30 eV) over $Au_{10}Co_9@Pt_{60}$ NC. This further suggests that $Au_{10}Co_9@Pt_{60}$ NC is a selective catalyst for H_2O_2 formation.

***H_2O formation:**

*OH can undergo hydrogenation (step 7) towards the formation of *H_2O. The calculated activation barriers for this step are 0.20, 0.39 and 0.12 eV on the $Co_{19}@Pt_{60}$, $Au_{19}@Pt_{60}$ and $Au_{10}Co_9@Pt_{60}$ NCs, respectively. Our results show that the *H_2O formation is more favourable on pure NC than that on core-shell NCs. Among core-shell NCs, $Au_{10}Co_9@Pt_{60}$ requires lowest activation barrier (0.12 eV) for H_2O formation. However, *OH formation (step 3/4/6) requires

View Article Online
DOI: 10.1039/C7NR03002A

high activation barrier on $Au_{10}Co_9@Pt_{60}$ NC. Therefore, H_2O formation will not be a favourable process on $Au_{10}Co_9@Pt_{60}$ NC.

It is very interesting to find out the trend in reaction free energy for $*H_2O$ formation (step 7). The elementary step is a highly exergonic when Co is used as a core metal and it is slight exergonic when Au is used. In case of mixed core, the reaction free energy value lies in between. The trend is very much in agreement as proposed by Nørskov et al.[32], where the binding energy of *O and *OH has been used as a descriptor for catalyst activity. Interestingly, our NCs model show similar trend as found in the periodic alloy surface based models.

Therefore, after careful investigation on all the possible elementary steps (Scheme 1), we find that *OOH hydrogenation step is the rate determining step on the $Au_{10}Co_9@Pt_{60}$ NC with an activation barrier of 0.46 eV, which is far lower than the previously reported activation barriers on the periodic Pd(111), Au(111) and Pd-Au(111) surfaces. Hence, $Au_{10}Co_9@Pt_{60}$ NC could be a potential candidate for direct H_2O_2 synthesis. Furthermore, it is noteworthy to mention that reaction free energy and activation doesn't run in parallel way (Scheme 1) in four cases such as: $*O_2$ dissociation ($*O_2 \rightarrow *O + *O$), *OOH dissociation ($*OOH \rightarrow *O + *OH$), $*H_2O_2$ dissociation ($*H_2O_2 \rightarrow *OH + *OH$) on $Au_{19}@Pt_{60}$ NC and $*H_2O_2$ formation ($*OOH + *H \rightarrow *H_2O_2$) on $Au_{10}Co_9@Pt_{60}$ NC. It is very interesting to find the trend that all the O-O dissociation process dissociation process is not favoured on $Au_{19}@Pt_{60}$. This is due to the less charge transfer to π^*-orbital of adsorbed oxygenated species, which renders the O-O bond dissociation on $Au_{19}@Pt_{60}$ NC. Another key point is that $*H_2O_2$ formation requires a high activation barrier though the reaction is exergonic and the underlying reason is as following. For OH formation ($*O + *H \rightarrow *OH$), we find that the transition state has a product like structure, whereas for $*H_2O_2$ formation ($*H + *OOH \rightarrow *H_2O_2$), TS has a reactant like structure. In the TS of $*H_2O_2$

View Article Online
DOI: 10.1039/C7NR03002A

formation, *H prefers to occupy at the bridge site of NC's facet, which is not a stable site for *H adsorption. This is the reason for high-energy barrier for $*H_2O_2$ formation though the reaction is thermodynamically favourable.

Moreover, we have studied the four important steps of H_2O_2 formation ($*O_2$ dissociation, *OOH formation, *OOH dissociation and $*H_2O_2$ formation steps) at the low-coordinated edge site to compare the two-electron reduction activity with respect to (111) facet. The calculated activation barriers for these have been given in Table S5. Our results show that direct $*O_2$ dissociation step ($*O_2 \rightarrow *O + *O$) is very much favourable on the (111) facet and edge sites of the NC. However, the *OOH formation ($*O_2 + *H \rightarrow *OOH$) requires a very high barrier (0.44 eV) at the edge site and therefore decreases the possibility of H_2O_2 formation. Moreover, unlike at the facet site, the OOH dissociation ($*OOH \rightarrow *O + *OH$) is very much favourable at the edge sites. In fact, we could not locate the transition state and might be undergoing via a barrierless pathway. We have carefully examined the structural parameters of the intermediates to find out the underlying reason behind this. We find that the O-O bond distance in *OOH is very high (1.50 Å) while adsorbed at the edge site than while adsorbed on the (111) facet (1.44 Å). The longer O-O bond distance at the edge is due to the higher unsaturation at the edge site, where the two O-atoms of OOH bonds directly bonded to two Pt atoms. Therefore, the elongated O-O bond distance is the underlying reason for facile *OOH dissociation. However, H_2O_2 formation ($*OOH + *H \rightarrow *H_2O_2$) requires a low barrier (0.24 eV) at the edge site compared to that on the (111) facet (0.46 eV). Lower barrier of $*H_2O_2$ formation can be understood from the strong binding energy of $*H_2O_2$ at the edge sites (-0.38 eV) compared to facet sites (-0.28 eV). Therefore, the reaction kinetics is very much dependent on the reaction sites. However, low coordinates sites of $Au_{10}Co_9@Pt_{60}$ NC are not active for H_2O_2 formation.

View Article Online
DOI: 10.1039/C7NR03002A

In addition, we have calculated reaction free energies and activation barriers for two important H_2O_2 formation steps on the $Au_9Co_9Pt_1@Au_1Pt_{59}$ (Au-segregated NC), as there is a possibility of inter-conversion from $Au_{10}Co_9@Pt_{60}$ to $Au_9Co_9Pt_1@Au_1Pt_{59}$ NC (Figure S4). Our results (Table S6) show that reaction free energies and activation barriers for H_2O_2 formation on the $Au_9Co_9Pt_1@Au_1Pt_{59}$ NC is very much comparable with the $Au_{10}Co_9@Pt_{60}$ and thus we can say that $Au_{10}Co_9@Pt_{60}$ NC is an excellent candidate for direct H_2O_2 synthesis.

3.3 Reaction mechanism on periodic surface:

We have compared the adsorption energies (Table S7) of the intermediate species on the periodic AuCo@Pt(111) surface and on the $Au_{10}Co_9@Pt_{60}$ NC. We have found that the preferred binding sites are the same for all of the adsorbates on both the surfaces (Table S7). It is interesting to find out that most of the intermediates are adsorbed weakly on the periodic AuCo@Pt(111) surface compared to that for a $Au_{10}Co_9@Pt_{60}$ NC. Therefore, periodic AuCo@Pt(111) surface shows interesting behaviour compared to the nanocluster model ($Au_{10}Co_9@Pt_{60}$ NC).

We have calculated reaction free energies and activation barriers (Table 2) for four important steps of H_2O_2 formation ($*O_2$ dissociation, *OOH formation, *OOH dissociation and $*H_2O_2$ formation) on the periodic AuCo@Pt(111) surface also. Our calculated reaction free energies and activation barriers show that $*O_2$ dissociation ($*O_2 \rightarrow *O + *O$) and *OOH formation ($*O_2 + *H \rightarrow *OOH$) steps are very much comparable with that of cluster model. Interestingly, *OOH dissociation step ($*OOH \rightarrow *O + *OH$) is very favourable (0.26 eV) on the periodic surface than that on the cluster model (0.61 eV). Moreover, the barrier for H_2O_2 is very high (0.90 eV) on the slab model than that on the cluster model (0.46 eV). This suggests that core-shell based $Au_{10}Co_9@Pt_{60}$ NC is very much efficient and selective catalyst for H_2O_2 formation compared to slab model.

View Article Online
DOI: 10.1039/C7NR03002A

Table 2: Reaction free energies (in eV) and activation barriers (in eV, parenthesis) on periodic AuCo@Pt(111) surface and $Au_{10}Co_9@Pt_{60}$ NC.

Elementary steps	Periodic AuCo@Pt(111) surface	$Au_{10}Co_9@Pt_{60}$
$*O_2 \rightarrow *O + *O$	-1.25 (0.11)	-2.27 (0.06)
$*O_2 + *H \rightarrow *OOH$	-0.41 (0.15)	-0.21 (0.12)
$*OOH \rightarrow *O + *OH$	-1.01 (0.26)	-1.79 (0.61)
$*OOH + *H \rightarrow *H_2O_2$	-0.45 (0.90)	-0.21 (0.46)

3.4 Effect of applied potential:

Our calculated activation barriers and reaction free energies for $4e^-$ and $2e^-$ reduction pathways suggest that $2e^-$ reduction is very much preferred over $Au_{10}Co_9@Pt_{60}$ NC. However, the role of electrode potential is very much important as ORR happens under an applied potential. Thus, these catalysts are exposed to electrical potential during the course of the electrochemical reaction. Therefore, the effects of electrode potential on reaction free energy and reduction mechanisms have been investigated as proposed by Nørskov and co-workers.[76] The free energy change (ΔG) is calculated as follows:

$$\Delta G = \Delta E + \Delta ZPE - T\Delta S - eU$$

where ΔE is the total energy change obtained from the DFT calculations, ΔZPE is the change in zero-point energy, T is the room temperature (300 K), ΔS is the entropy change, e is the transferred charge for the elementary step and U is the electrode potential with respect to the standard hydrogen electrode (SHE).

View Article Online
DOI: 10.1039/C7NR03002A

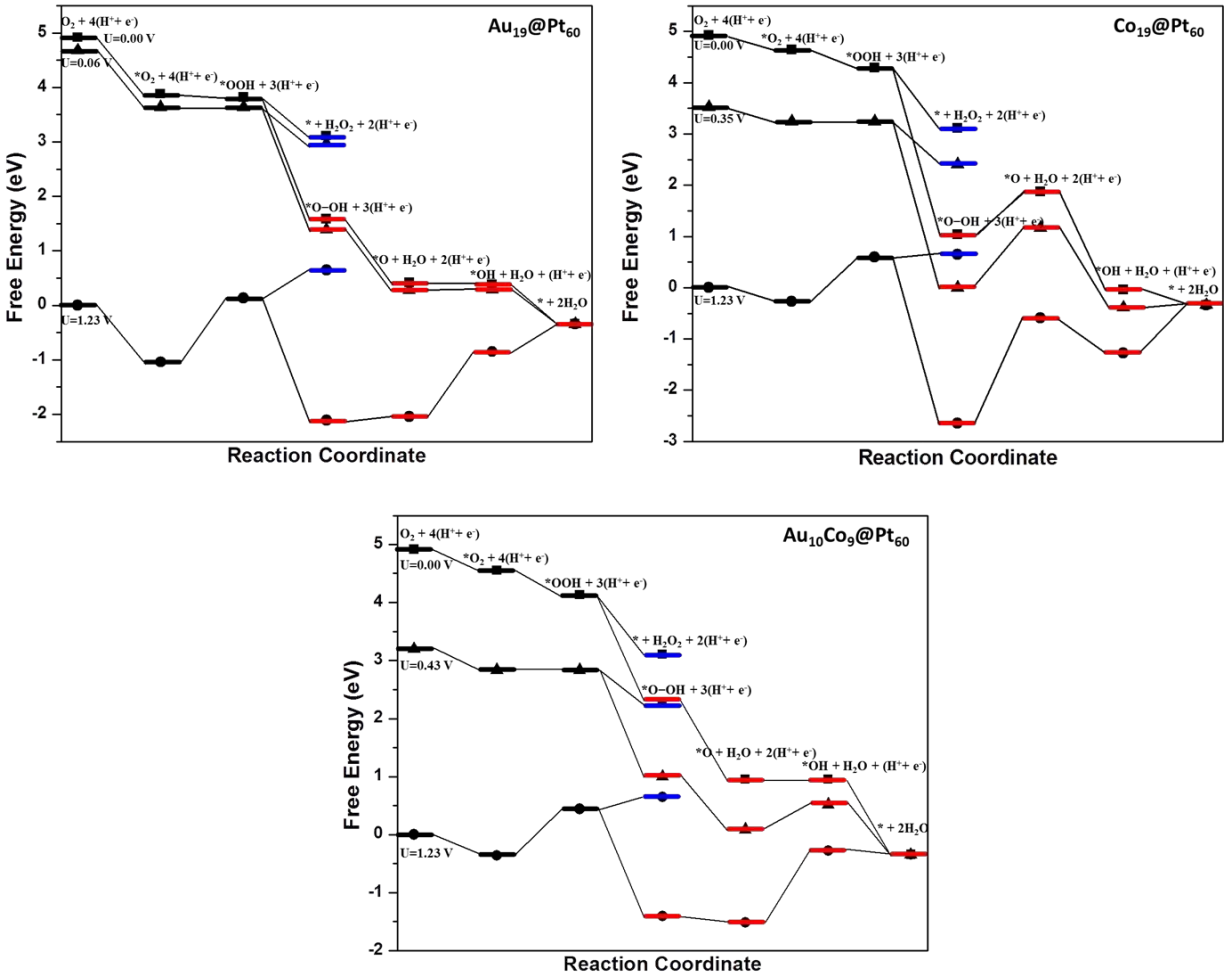

Figure 3: Free energy diagrams for ORR mechanism at different potentials. Here, blue and red lines represent the $2e^-$ and $4e^-$ reduction pathways, respectively.

Figure 3 shows that all the elementary steps are downhill process at U = 0 V irrespective of NCs. However, proton transfer steps are thermodynamically not favourable as we increase the applied potential. Figure 3 shows that all $2e^-$ reduction steps (*OOH and H_2O_2 formation) are exergonic under highest electrode potential of 0.06, 0.35 and 0.43 V on $Co_{19}@Pt_{60}$, $Au_{19}@Pt_{60}$ and $Au_{10}Co_9@Pt_{60}$, respectively. Therefore, $Au_{10}Co_9@Pt_{60}$ NC is a better catalyst than $Co_{19}@Pt_{60}$ and $Au_{19}@Pt_{60}$ NC for H_2O_2 production. Therefore, the working potential (0.43 V) is very much close to the equilibrium potential (0.69 V) of $2e^-$ reduction on $Au_{10}Co_9@Pt_{60}$. So such

View Article Online
DOI: 10.1039/C7NR03002A

$Au_{10}Co_9@Pt_{60}$NC substantially lowers the overpotential. Furthermore, *OH formation becomes endergonic at 0.43 V when catalyzed by $Au_{10}Co_9@Pt_{60}$ NC, which indicates the absence of any competitive $4e^-$ reduction pathway. Therefore, H_2O formation is not favourable on the $Au_{10}Co_9@Pt_{60}$ NC and thus very selective towards H_2O_2 formation. Furthermore, the free energy profile of $Co_{19}@Pt_{60}$ NC clearly shows that it does not favour H_2O_2 formation. The *OH formation step is a downhill process even at 1.23 V on $Co_{19}@Pt_{60}$, which suggests that they catalyst may favour H_2O formation over H_2O_2 formation. Therefore, despite a high working potential (0.35 V) for H_2O_2 production, $Co_{19}@Pt_{60}$ NC suffers low selectivity towards H_2O_2 formation. On the other hand, the O_2 hydrogenation step becomes endergonic above 0.06 V on $Au_{19}Pt_{60}$ NC and thus it does not favour H_2O_2 formation. Therefore, our free energy diagrams support our conclusion drawn from activation barrier values that $Au_{10}Co_9@Pt_{60}$ NC is very much efficient and selective towards H_2O_2 formation.

4. Conclusion:

First-principles calculations are performed to understand the role of core metal in core-shell NCs towards $2e^-$ ORR over $4e^-$ ORR. This is very important to understand the product selectivity (H_2O vs. H_2O_2). The cuboctahedral Pt_{79}, $Au_{19}@Pt_{60}$, $Co_{19}@Pt_{60}$ and $Au_{10}Co_9@Pt_{60}$ NCs enclosed by well-defined facets have been chosen for our study. Reaction free energies and activation barriers are calculated for all the possible elementary steps of $4e^-$ and $2e^-$ reduction process on the (111) facet of the NCs. Our calculated activation barriers show that $Au_{10}Co_9@Pt_{60}$ NC is very much efficient and selective towards H_2O_2 formation. Our comparisons with previous studies on periodic surface [Pd(111), Au(111)] and alloy-based Pd-Au(111)] based catalysts show that rate determining steps of H_2O_2 formation are significantly improved over the NCs than that on any other catalyst reported so far. The preference of O_2 hydrogenation over O_2 dissociation can be

View Article Online
DOI: 10.1039/C7NR03002A

explained based on the charge transfer than the adsorption behaviour of O_2. This is very much different from the previous ORR studies on alloy-based Pt(111) surface, where the Pt-O bonding nature has been attributed for O-O bond dissociation mechanism. Moreover, $Au_{10}Co_9@Pt_{60}$ NC is found to be a promising catalyst for H_2O_2 formation via the much desired Langmuir-Hinshelwood mechanism due to the very feasible dissociative adsorption behaviour of H_2 molecule on the catalyst surface. Furthermore, the potential dependent free energy study suggests that the H_2O_2 formation is thermodynamically favourable up to 0.43 V on $Au_{10}Co_9@Pt_{60}$ NC and thus significantly lowers the overpotential for $2e^-$ ORR process. In fact, the *OH formation step becomes non-spontaneous at 0.43 V potential, thus indicating the absence of any competitive $4e^-$ reduction pathway. Therefore, the $Au_{10}Co_9@Pt_{60}$ NC is very much selective towards H_2O_2 formation over H_2O formation.

Supporting Information:

The followings have been provided in the Supporting Information. Model of periodic AuCo@Pt(111) surface, optimized geometry and segregation energy of the NCs, computational details, adsorption behaviours of the intermediates on $Au_{10}Co_9@Pt_{60}$ NC, adsorption energies of the reaction intermediates and reaction free energies on $Au_{10}Co_9@Pt_{60}$ NC at edge and facet sites, rate constants values for the elementary reactions at 300 K on different NCs, adsorption behaviours and reaction energetics of the H_2O_2 synthesis and adsorption energies (in eV) of the reaction intermediates on periodic AuCo@Pt(111) surface and $Au_{10}Co_9@Pt_{60}$ NC.

Acknowledgments

We thank IIT Indore for the lab and computing facilities. This work is financially supported by DST-SERB (EMR/2015/002057).

View Article Online
DOI: 10.1039/C7NR03002A

References:

[1] J. M. Campos-Martin, G. Blanco-Brieva and J. L. G. Fierro, *Angew. Chem., Int. Ed.,* 2006, **45**, 6962−6984.

[2] C. Samanta, *Appl. Catal., A,* 2008, **350**, 133−149.

[3] J. Van Weynbergh, J. P. Schoebrechts and J. C. Colery *U.S. Patent*, 1992, **5447706**.

[4] J. K. Edwards, B. Solsona, E. N. N, A. F. Carley, A. A. Herzing, C. J. Kiely and G. J. Hutchings, *Science,* 2009, **323**, 1037−1041.

[5] N. E. Ntainjua, J. K. Edwards, A. F. Carley, J. A. Lopez-Sanchez, J. A. Moulijn, A. A. Herzing, C. J. Kiely and G. J. Hutchings, *Green Chem.*, 2008, **10**, 1162–1169.

[6] S. Siahrostami, A. Verdaguer-Casadevall, M. Karamad, D. Deiana, P. Malacrida, B. Wickman, M. Escudero-Escribano, E. A. Paoli, R. Frydendal and T. W. Hansen, *Nat. Mater.* 2013, **12**, 1137−1143.

[7] A. Verdaguer-Casadevall, D. Deiana, M. Karamad, S. Siahrostami, P. Malacrida, T. W. Hansen, J. Rossmeisl, I. Chorkendorff and I. E. L. Stephens, *Nano Lett*., 2014, **14**, 1603−1608.

[8] T. P. Fellinger, F. Hasche, P. Strasser and M. Antonietti, *J. Am. Chem. Soc*., 2012, **134**, 4072−4075.

[9] J. Park, Y. Nabae, T. Hayakawa, M. A. Kakimoto, *ACS Catal.,* 2014, **4**, 3749−3754.

[10] A. Mahata, K. S. Rawat, I. Choudhuri and B. Pathak, *J. Mater. Chem. A,* 2016, **4**, 12756−12767.

[11] F. Gao and D. W. Goodman, *Chem. Soc. Rev.,* 2012, **41**, 8009–8020.

[12] J. S. Jirkovsky, I. Panas, E. Ahlberg, M. Halasa, S. Romani and D. J. Schiffrin, *J. Am. Chem. Soc*., 2011, **133**, 19432−19441.

[13] J. Li and K. Yoshizawaa, *Catal. Today*, 2015, **248**, 142–148.

View Article Online
DOI: 10.1039/C7NR03002A

[14] H. C. Ham, G. S. Hwang, J. Han, S. W. Nam and T. H. Lim, *J. Phys. Chem. C,* 2010, **114**, 14922–14928.

[15] J. Li, T. Ishihara and K. Yoshizawa, *J. Phys. Chem. C,* 2011, **115**, 25359–25367.

[16] H. C. Ham, G. S. Hwang, J. Han, S. W. Nam and T. H. Lim, *J. Phys. Chem. C,* 2009, **113**, 12943–12945.

[17] J. Li, A. Staykov, T. Ishihara and K. Yoshizawa, *J. Phys. Chem. C,* 2011, **115**, 7392–7398.

[18] A. V. Beletskaya, D. A. Pichugina, A. F. Shestakov and N. E. Kuzmenko, *J. Phys. Chem. A*, 2013, **117**, 6817−6826.

[19] P. J. Collier, A. F. Carley, D. Chadwick, A. J. Papworth, A. Burrows, C. J. Kiely and G. J. Hutchings, *Phys. Chem. Chem. Phys*., 2003, **5**, 1917–1923.

[20] J. K. Edwards, B. Solsona, P. Landon, A. F. Carley, A. Herzing, M. Watanabe, C. J. Kiely and G. J. Hutchings, *J. Mater. Chem*., 2005, **15**, 4595–4600.

[21] V. R. Choudhary and P. Jana, *J. Catal.,* 2007, **246**, 434-439.

[22] E. Antolinia, *Energy, Environ. Sci*., 2009, **2**, 915-931.

[23] A. C. Garcia, V. A. Paganin and E. A. Ticianelli, *Electrochim. Acta*, 2008, **53**, 4309-4315.

[24] Y. H. Cho, B. Choi, Y. H. Cho, H. S. Park and Y. E. Sung, *Electrochem. Commun*., 2007, **9**, 378-381.

[25] T. Deguchi and M. Iwamoto, *J. Phys. Chem. C,* 2013, **117**, 18540−18548.

[26] Z. Duan and G. A Wang, *Phys. Chem. Chem. Phys.*, 2011, **13**, 20178–20187.

[27] K. Li, Y. Li, Y. Wang, F. He, M. Jiao, H. Tang and Z. Wu, *J. Mater. Chem. A,* 2015, **3**, 11444−11452.

[28] L. Ou and S. Chen, *J. Phys. Chem. C,* 2013, **117**, 1342−1349.

[29] S. Kattel, Z. Duan, G. Wang, *J. Phys. Chem. C,* 2013, **117**, 7107−7113.

View Article Online
DOI: 10.1039/C7NR03002A

[30] A. Mahata, P. Bhauriyal, K. S. Rawat and B. Pathak, *ACS Energy Lett.,* 2016, **1**, 797−805.

[31] T. Deguchi, H. Yamano, S. Takenouchi and M. Iwamoto, *Catal. Sci. Technol*., 2016, **6**, 4232-4242.

[32] J. Greeley, I. E. L. Stephens, A. S. Bondarenko, T. P. Johansson, H. A. Hansen, T. F. Jaramillo, J. Rossmeisl, I. Chorkendorff and J. K. Nørskov, *Nat. Chem*., 2009, **1**, 552 – 556.

[33] I. E. L. Stephens, A. S. Bondarenko, U. Grønbjerg, J. Rossmeisl and I. Chorkendorff, *Energy Environ. Sci.*, 2012, **5**, 6744-6762.

[34] V. R. Stamenkovic, B. S. Mun, K. J. J. Mayrhofer, P. N. Ross and N. M. Markovic, *J. Am. Chem. Soc*., 2006, **128**, 8813−8819.

[35] C. Wang, M. Chi, D. Li, D. Strmcnik, D. van der Vliet, G. Wang, V. Komanicky, K. Chang, A. P. Paulikas, D. Tripkovic, J. Pearson, K. L. More, N. M. Markovic and V. R. Stamenkovic, *J. Am. Chem. Soc.,* 2011, **133**, 14396−14403.

[36] W. J. Tang, L. Zhang and G. Henkelman, *J. Phys. Chem. Lett*., 2011, **2**, 1328−1331.

[37] J. X. Wang, H. Inada, L. Wu, Y. Zhu, Y. Choi, P. Liu, W. P. Zhou and R. R. Adzic, *J. Am. Chem. Soc.,* 2009, **131**, 17298−17302.

[38] (a) R. G. Chaudhuri and S. Paria, *Chem. Rev.,* 2012, **112,** 2373-2433. (b) M. B. Gawande, A. Goswami, T. Asefa, H. Guo, A. V. Biradar, D-L Peng, R. Zboril and R. S. Varma, *Chem. Soc. Rev.,* 2015, **44,** 7540-7590. (c) J-F Li, Y-J Zhang, S-Y Ding, R. Panneerselvam and Z-Q Tian, *Chem. Rev.,* 2017, **117,** 5002-5069.

[39] V. R. Stamenkovic, B. Fowler, B. S. Mun, G. Wang, P. N. Ross, C. A. Lucas and N. M. Marković, *Science*, 2007, **315**, 493−497.

[40] V. Stamenkovic, B. S. Mun, K. J. J. Mayrhofer, P. N. Ross, N. M. Markovic, J. Rossmeisl, J. Greeley and J. K. Nørskov, *Angew. Chem*., 2006, **118**, 2963−2967.

View Article Online
DOI: 10.1039/C7NR03002A

[41] (a) B. Zhang, D. Wang, Y. Hou, S. Yang, X. H. Yang, J. H. Zhong, J. Liu, H. F. Wang, P. Hu, H. J. Zhao and H. G. Yang, *Scientific Reports,* 2013, **3,** 1836. (b) Y. Hu, H. Zhang, P. Wu, H. Zhang, B. Zhou and C. Cai, *Phys. Chem. Chem. Phys.,* 2011, **13,** 4083-4094. (c) S. Ghosh, R. K. Sahu and C. R. Raj, *Nanotechnology,* 2012, **23,** 385602. (d) T. Maiyalagan and F. N. Khan, *Catal. Comm.,* 2009, **10,** 433-436. (e) H-W. Ha, I. Y. Kim, S-J. Hwang and R. S. Ruoff, *Electrochem. Solid State Lett.,* 2011, **14,** B70.

[42] J. Wu, J. Zhang, Z. Peng, S. Yang, F. T. Wagner and H. Yang, *J. Am. Chem. Soc.,* 2010, **132,** 4984-4985.

[43] C. M. Sánchez-Sánchez, J. Solla-Gullón, F. J. Vidal-Iglesias, A. Aldaz, V. Montiel and E. Herrero, *J. Am. Chem. Soc.,* 2010, **132,** 5622-5624.

[44] (a) Dr. G. Collins, M. Schmidt, Dr. C. O'Dwyer, Prof. J. D. Holmes and Dr. G. P. McGlacken, *Angew. Chem., Int. Ed.,* 2014, **53,** 4142-4145. (b) M. Jin, H. Zhang, Z. Xieb and Y. Xia, *Energy Environ. Sci.,* 2012, **5,** 6352-6357, (c) C. Wang, H. Daimon, T. Onodera, T. Koda, and S. Sun, Angew. Chem., Int. Ed., 2008, 47, 3588-3591.

[45] A. Mahata, K. S. Rawat, I. Choudhuri and Pathak, B. *Catal. Sci. Technol.*, 2016, **6,** 7913-7923.

[46] H. M. Song, D. H. Anjum, R. Sougrat, M. N. Hedhilib and N. M. Khashab, J. Mater. Chem., 2012, 22, 25003-25010.

[47] (a) J-Y. Bigot, H. Kesserwan, V. Halté, O. Ersen, M. S. Moldovan, T. H. Kim, J-t. Jang and J. Cheon, *Nano Lett.,* 2012, **12,** 1189-1197. (b) L. Wanga, Z. Tanga, W. Yana, Q. Wanga, H. Yanga and S. Chena, *J. of Power Sources,* 2017, **343,** 458-466.

[48] L-L. Wang and D. D. Johnson, *J. Am. Chem. Soc.,* 2009, **131,** 14023–14029.

[49] H. A. Gasteiger and P. N. Ross, *J. Phys. Chem.,* 1996, **100**, 6715−6721.

View Article Online
DOI: 10.1039/C7NR03002A

[50] N. Tian, Z. Y. Zhou, S. G. Sun, Y. Ding, Z. L. Wang, *Science*, 2007, **316**, 732−735.

[51] B. Han, V. Viswanathan and H. Pitsch, *J. Phys. Chem. C,* 2012, **116**, 6174−6183.

[52] J. Solla-Gullon, F. J. Vidal-Iglesias, A. Lopez-Cudero, E. Garnier, J. M. Feliu and A. Aldaz, *Phys. Chem. Chem. Phys*., 2008, **10**, 3689−3698.

[53] P. E. Blochl, *Phy. Rev. B,* 1994, **50**, 17953.

[54] G. Kresse, Hafner, *J. Phy. Rev. B,* 1993, **47**, 558.

[55] G. Kresse, Hafner, *J. Phy. Rev. B,* 1994, **49**, 14251.

[56] G. Kresse and D. Joubert, *Phy. Rev. B,* 1999, **59**, 1758.

[57] J. P. Perdew, J. A. Chevary, S. H. Vosko, K. A. Jackson, M. R. Pederson, D. J. Singh and C. Fiolhais, *Phy. Rev. B,* 1992, **46**, 6671.

[58] S. Grimme, J. Antony, S. Ehrlich, S. Krieg, *J. Chem. Phys.,* 2010, **132**, 154104.

[59] G. Henkelman and H. Jonsson, *J. Chem. Phys.,* 2000, **113**, 9978-9985.

[60] L. Qi, X. Qian and J. Li, *Phys. Rev. Lett.,* 2008, **101**, 146101

[61] J. A. Keith, G. Jerkiewicz and T. Jacob, *ChemPhysChem*, 2010, **11**, 2779-2794.

[62] Z. Lin, T. Chou, C. Liu, P. Huang, Y. Guo, J. Wang and K. Wang, *J. Mater. Chem. A*, 2016, **4**, 11023–11029.

[63] P. C. Jennings, H. A. Aleksandrov, K. M. Neyman and R. L. Johnston, *J. Phys. Chem. C,* 2015, **119**, 11031−11041.

[64] L. Pauling, *Cornell Univ., USA, 3rd ed.,* 1960.

[65] H. Xu, D. Cheng and Y. Gao, *ACS Catal.,* 2017, **7,** 2164−2170.

[66] J. Zhang, K. Sasaki, E. Sutter and R. R. Adzic, *Science,* 2007, **315,** 220-222.

[67] S. S. Kumar and K. L. N. Phani, *J. of Power Sources,* 2009, **187,** 19-24.

[68] L. An, W. Huang, N. Zhang, X. Chenc and D. Xia, *J. Mater. Chem. A,* 2014, **2,** 62-65.

View Article Online
DOI: 10.1039/C7NR03002A

[69] D. C. Ford, A. U. Nilekar, Y. Xu and M. Mavrikakis, *Sur. Sci*., 2010, **604**, 1565–1575.

[70] R. Todorovic, R. J. Meyer, Catal. Today 2011, 160, 242−248

[71] T. Ishiharaa, Y. Ohurab, S. Yoshidab, Y. Hataa, H. Nishiguchib and Y. Takitab, *App. Catal. A*, 2005, **291**, 215-221.

[72] J. Lia and K. Yoshizawa, *Catal. Today,* 2015, **248**, 142-148.

[73] J. R. Kitchin, J. K. Nørskov, M. A. Barteau and J. G. Chen, *Phys. Rev. Lett.,* 2004, **93**, 156801.

[74] L. Zhang and G. Henkelman, *J. Phys. Chem. C,* 2012, **116**, 20860−20865.

[75] S. Lin, K. Wang, C. Liu, H. Chen and J. Wang, *J. Phys. Chem. C,* 2015, **119**, 15224−15231.

[76] J. K. Nørskov, J. Rossmeisl, A. Logadottir, L. Lindqvist, J. R. Kitchin, T. Bligaard and H. Jonsson, *J. Phys. Chem. B,* 2004, **108**, 17886-17892.

View Article Online
DOI: 10.1039/C7NR03002A

Table of Content: